Journal Name

ARTICLE

Surfactant-assisted ZnO processing as a versatile route to ZIF composites and hollow architectures with enhanced dye adsorption

Received 00th January 20xx,
Accepted 00th January 20xx

DOI: 10.1039/x0xx00000x

www.rsc.org/

Samir El-Hankari[a†], Jordi Aguilera-Sigalat[a†] and Darren Bradshaw*[a]

Metal oxides can be used as hard sacrificial templates for the preparation of multifunctional core-shell MOF-based composites following reaction with the organic linker. This is a facile method, but often structures of well-defined shape are only obtained under narrow ranges of conditions, the shape can be lost completely and low levels of MOF conversion observed. Using the prototypical framework ZIF-8 we present an alternative surfactant-assisted surface passivation strategy where the ZnO precursor particles are first coated with a guanidinium-based amphiphile. The surfactant interacts strongly with the oxide surface and allows fine-tuning of the release of Zn(II) and ZIF-8 nucleation by the level of surface coverage permitting a range of well-defined ZnO@ZIF-8 core-shell architectures to be prepared including in water. Further, selective base-etching of the oxide core provides facile access to hollow ZIF-8 and yolk-shell structures. We also demonstrate enhanced dye adsorption and recovery from aqueous mixtures using ZnO@ZIF-8 composite microspheres..

Introduction

Over the last decade metal-organic frameworks (MOFs)[1] constructed by coordination interactions between metal ions and organic linkers have fully established themselves as an exciting class of high-surface area microporous materials of tuneable functionality with wide-ranging applications in catalysis[2], separation[3], energy[4] and drug delivery[5] with further potential in a number of emerging areas such as biotechnology and microelectronics[6]. While these applications strongly depend on the composition and structure of the MOF, it is clear that their properties can be significantly enhanced through appropriate configuration of the physical form of the MOFs[7] or the preparation of MOF-based composite materials[8]. Metal oxides (MOs) are a particularly effective starting point to realise these goals, acting as hard templates for the preparation of a range of supported MOF membranes[9], core-shell structures[10] and higher-level architectures through pseudomorphic replacement strategies[11]. Metal oxide particles can also be used to seed the growth of MOFs allowing crystals of MOFs to be deposited in precise locations[12]. In many cases the properties of the MO@MOF composites are enhanced, with the oxide component endowing the frameworks with magnetic, optical or catalytic properties and the MOF providing a functional and size-selective shell[10, 13].

Owing to its chemical and thermal stability and high surface area that are desirable for many applications, tetrahedrally-connected ZIF-8 [$Zn(MeIm_2)$] (where MeIm = 2-methylimidazole)[14] has been widely prepared from the corresponding ZnO.[15] For example, ZnO nanorods and layers have been employed for the deposition of ZIF-8 and patterned ZIF-8 thin films[16], including by a MOF chemical vapour deposition technique permitting ZIF-8 to be deposited in a highly controlled and uniform way on well-defined surface-supported ZnO features[17].

Core-shell ZnO@ZIF-8 composites are also readily accessible, and such materials have been exploited for size-selective photocatalysis due to the semiconductor properties of ZnO especially for the breakdown of dye molecules for applications in bioremediation[18]. The ZnO@ZIF-8 composites have also been used as sensors where bulk core-shell nanorods can be used for the selective electrochemical detection of volatile organic compounds including formaldehyde[19], and ZnO@ZIF-8 nanorod arrays for the photoelectrochemical detection of hydrogen peroxide[20]. Pd nanoparticles supported on ZnO microspheres have also been employed to prepare Pd/ZnO@ZIF-8 core-shell composites for the size-selective catalytic hydrogenation of alkenes[21].

When ZnO is exposed to solutions of MeIm the organic plays two roles, acting simultaneously as etchant to release Zn(II) ions from the oxide which itself acts as a sacrificial template[22] and permits coordination to those ions for ZIF-8 assembly. For the preparation of well-defined ZnO@ZIF-8 core shell structures however, it is understood that the correct balance between the rates of Zn(II) release and coordination are required to promote heterogeneous nucleation on the oxide template rather than homogeneous nucleation in solution.[18a,22] This can be controlled to an extent[18-22] by choice

[a] School of Chemistry, University of Southampton, Highfield Campus, Southampton, U.K. E-mail: D.Bradshaw@soton.ac.uk
†Electronic Supplementary Information (ESI) available: []. See DOI: 10.1039/x0xx00000x

of solvent or by modulating the concentration of MeIm, although

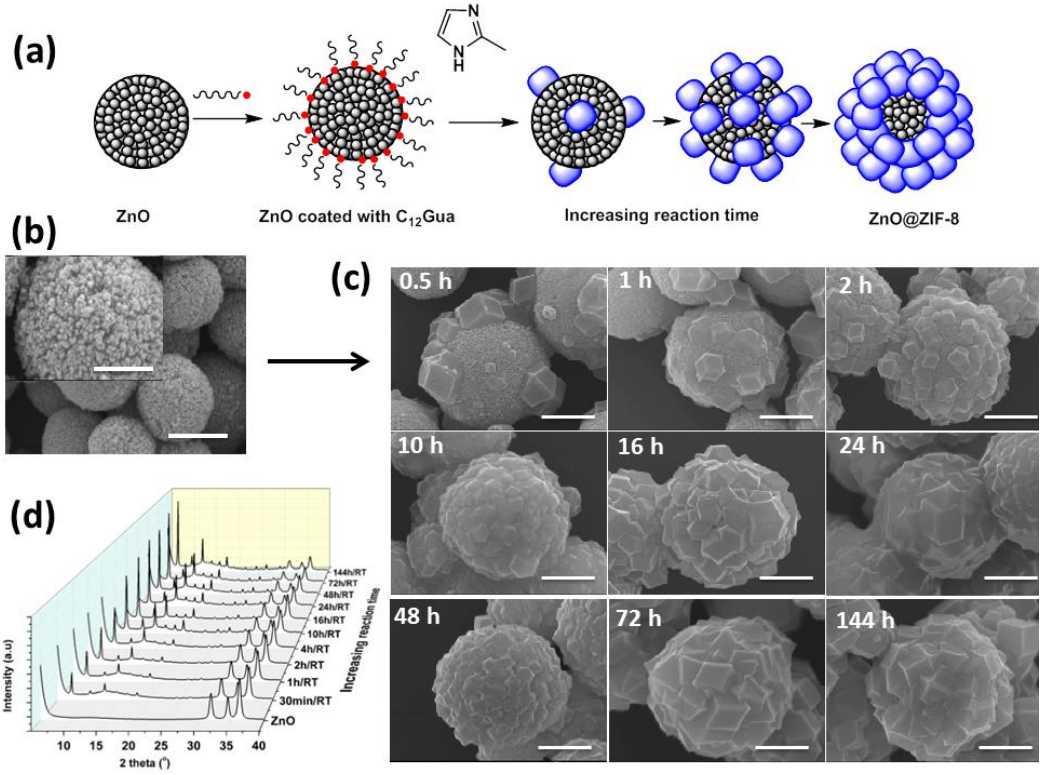

Figure 1. (a) Schematic representation of the preparation of ZnO@ZIF-8 core-shell microspheres in the presence of a C_{12}Gua surfactant. (b) SEM images of the mesoporous ZnO microsphere template, scale bars = 1 µm and 0.5 µm (inset). (c) SEM images of surface coverage of ZnO microspheres with ZIF-8 crystals following various reaction times with MeIm in MeOH at rt; all scale bars = 1 µm. (d) Stack plot of PXRD data of ZnO microspheres and the resulting ZnO@ZIF-8 composites at reaction times corresponding to those in (c).

it is noted that often only a very narrow range of conditions give rise to only the desired core-shell structures. Further, conversion rates of oxide to ZIF can also be rather low as a consequence of balancing these parameters. The size and shape of the resulting ZIF-8 can also be quite different from those of the starting ZnO precursors especially when these are at the nanoscale[23], which for templating is highly undesirable.

In this contribution we outline an oxide surface passivation strategy as an alternative method to fine-tune the balance between Zn(II) release and coordination rates and overcome some of the issues surrounding conversion level and template shape retention during composite formation. We use a guanidinium-based surfactant to coat the surface of the ZnO template particles where Zn(II) release and ZIF-8 nucleation can be regulated by the degree of guanidinium surface coverage, whose presence is crucial to the formation of well-defined ZnO@ZIF-8 core-shell micro- and nanospheres, nanowires and star-shaped architectures. The method is applicable under a range of experimental conditions, including in pure water. Using this strategy it is also straightforward to incorporate functional nanoparticles into the composites and we show that the oxide cores can be selectively etched away to leave hollow ZIF-8 and yolk-shell structures. Further we demonstrate the potential of the ZnO@ZIF-8 composite core-shell microspheres in the selective adsorption and recovery of rhodamine B from aqueous dye mixtures.

Results and discussion

Our developed synthetic methodology first involves the preparation and characterisation of mesoporous ZnO microspheres, which are subsequently transformed into ZnO@ZIF-8 composite materials after pre-coating in a guanidinium-based surfactant through a sacrificial template type methodology upon reaction with 2-methylimidazole (MeIm). (Figure 1a) The ZnO particles were synthesised using a starch-based aqueous solution method[24], followed by calcination at 500 °C. Scanning electron microscopy (SEM) reveals that microspheres of *c.a.* 1.5 µm diameter are formed, which are composed of aggregated 20 – 30 nm Wurtzite-type ZnO nanoparticles. (Figure 1b,d) The presence of textural mesoporosity in the ZnO microspheres is confirmed by a type IV nitrogen isotherm. (Figure S1)

Reaction of the ZnO microspheres with MeIm to form ZnO@ZIF-8 composites was carried out in MeOH, initially at room temperature (rt). The ZnO spheres were first stabilised by coating in dodecylguanidinium hydrochloride (C_{12}Gua), which was found to play an important role in the formation of the ZnO@ZIF-8 composites. Figure 1c shows SEM images of the ZnO@ZIF-8 composites formed using a Zn:MeIm molar

ratio of 1:30 with 0.27 mmol of C_{12}Gua at various reaction times. It is clear that the coverage of the ZnO microspheres with ZIF-8 increases with reaction time, starting from a few isolated crystals after 30 mins to the formation of a dense coating of intergrown ZIF-8 crystals after 10 hrs. Although the ZnO@ZIF-8 composite microspheres are too large to be effectively imaged by transmission electron microscopy (TEM), repeating the reaction in water with C_{12}Gua starting from ZnO nanospheres of 145 nm TEM clearly reveals a core-shell structure is formed where an increase in diameter following ZIF-8 growth is observed. (Figure S2) It is thus expected that following longer reaction times (> 10 hrs), the ZnO@ZIF-8 composite microspheres adopt a similar core-shell configuration.

Powder X-ray diffraction (PXRD) confirms the presence of both ZIF-8 and the oxide, with the relative intensity of the Bragg reflections associated with the latter decreasing with reaction time. (Figure 1d) Thermogravimetric analysis (TGA) reveals that conversion to ZIF-8 increases with reaction time (Figure S3, Table S1), from 17.2% after 1 hr reaching a level of 46.2% after 144 hrs under these conditions. The degree of conversion also slows as the reaction proceeds (Figure S4), particularly once the ZIF-8 shell is complete (~ 10 hrs), arising from an increased diffusion barrier to the reactive framework-forming components as the shell further thickens beyond this time[22].

The nitrogen adsorption data (Figure S5) follows a similar trend, where an overall increase in apparent BET surface area for the composite microspheres is found as the proportion of ZIF-8 increases (Table S1), from 310 m^2/g after 1 hr to 1106 m^2/g after 144 hrs of reaction, consistent with their composition. It is also noted that the rate of increase in the surface area slows with increasing reaction time, and the hysteresis loop associated with the mesoporous ZnO component diminishes over the same period as this is converted to microporous ZIF-8 and coverage of the shell becomes complete.

The proportion of ZIF-8 in the ZnO@ZIF-8 microspheres can be increased by raising the reaction temperature to 60 °C, reaching a maximum ZIF-8 conversion of 54.7% and a BET surface area of 1372 m^2/g for the composite following 144 hrs of reaction. (Figure S6-S8; Table S2) After 2 hrs of reaction time at this elevated temperature, the amount of ZIF-8 present is equivalent to 24 hrs at rt indicating a significantly increased rate of shell growth as diffusion effects are partly overcome by the increase in temperature. SEM images further reveal that the ZnO@ZIF-8 composites retain their microspherical morphology and that surface coverage increases with time as observed at rt. The ZIF-8 shell is largely complete after ~ 4 hrs at 60 °C. (Figure S9)

The C_{12}Gua surfactant appears to be critical for the composites to retain the microspherical shape of the starting ZnO (Figure 1c), since in its absence only bulk ZIF-8 crystals are observed. (Figure S10) Hence the role of the surfactant in the preparation of well-defined ZnO@ZIF-8 core-shell microspheres has been further studied, particularly at the earlier stages of composite formation. The degree of ZnO to ZIF-8 conversion is found to be strongly dependent on the amount of C_{12}Gua used: following 2 hrs of reaction at 60 °C for example, the degree of conversion with 0.18 mmol of added C_{12}Gua is 32.6%, compared with 51.0% with 1.08 mmol of the surfactant as confirmed by TGA. (Figure S11, S12; table S3) After 4 hrs of reaction it is also clear that the rate of conversion is accelerated as the amount of C_{12}Gua is increased, from an increase of 5.2% at 0.18 mmol to 9.8% at 1.08 mmol over that observed at 2 hrs.

The SEM images shown in figure S14 reveal a more complete ZnO surface coverage by smaller ZIF-8 crystals (150-200 nm) is achieved more quickly at the lowest concentrations of C_{12}Gua employed. When larger quantities of the surfactant are used however, each ZnO microsphere appears to act as a nucleation point for a smaller number of very large ZIF-8 crystals (1-2 μm), which decrease in number and increase in size as the concentration of C_{12}Gua increases leading to incomplete shell formation during the earlier stages of the reaction. (Figure S14) It is noted that at all levels of C_{12}Gua employed, the ZIF-8 shell appears to be complete after 4 hrs (Figure S14) consistent with previous observations at 60 °C. (Figure S9)

These results point strongly toward a surface passivation mechanism by the guanidinium-based surfactant, which regulates the release rate of Zn(II) in the presence of MeIm and controls the number of potential nucleation sites on the oxide surface. (Figure S15) When the concentration of C_{12}Gua is relatively low surface coverage of the oxide is sparse, leading to faster initial Zn(II) release and an abundance of nucleation points. This leads to a rapid deposition of ZIF-8 nanocrystals around the ZnO microspheres, which form a more complete shell earlier in the reaction. This early shell deposition provides a greater diffusion barrier and slows the subsequent growth rate leading to reduced overall conversion. At higher levels of C_{12}Gua, surface coverage of the ZnO microspheres is greater which slows Zn(II) release and reduces the number of nucleation points at the surface. This leads to a growth dominated deposition of ZIF-8 on the oxide, where a small number of large crystals that initially grow on the oxide reduce the overall diffusion barrier as shell formation is incomplete leading to higher conversion. By contrast, without C_{12}Gua significantly higher conversion of ZnO to bulk ZIF-8 is observed (Figure S16, S17) consistent with very rapid Zn(II) release and unrestricted homogeneous nucleation[23b].

A similar trend in conversion is seen when the concentration of the MeIm linker is modulated. (Figures S18-S21) Reducing the Zn:MeIm ratio leads to higher levels of ZnO to ZIF-8 conversion, ranging from 35.5% at a 1:30 ratio to 54.8% at 1:2 following reaction at 60°C for 72 hrs. (Figure S19; Table S4) This would *prima facie* seem counter-intuitive, but it is reasonable that when MeIm is present in a large excess there is a high initial concentration of the linker at the surface of the ZnO microspheres which further promotes Zn(II) release and more rapid shell deposition that increases the diffusion barrier for subsequent shell growth as observed for reducing the C_{12}Gua concentration. Previous studies[18a, 23a] report the importance of MeIm concentration and its role on balancing rates of Zn(II) release and coordination to obtain ZnO@ZIF-8 core-shell composites while limiting the amount of free ZIF-8

crystals, and typically only a very narrow range is appropriate. In the present case, well-defined core-shell composites and an absence of free ZIF-8 are observed at all levels of MeIm employed (figure S21), indicating that superior control is afforded with C_{12}Gua allowing conversion levels to ZIF-8 to be finely tuned.

We further investigated composite formation after pre-coating the ZnO particles in cetyl-trimethylammonium bromide (CTAB), a single chain cationic surfactant that has previously been reported to influence ZIF-8 crystal size and morphology in standard (solvothermal) syntheses from metal salts.[25] In the presence of CTAB the degree of ZnO to ZIF-8 conversion is 1.6 times higher than that obtained with C_{12}Gua under identical conditions, and SEM images indicate the microspherical shape is largely destroyed. (Figure S22, S23) This is in agreement with those composites prepared in the absence of any surfactant stabiliser (Figure S10, S16, S17) and suggests that CTAB does not interact as strongly as C_{12}Gua with the ZnO surface, further confirming the critical role of the guanidinium-based amphiphile in core-shell composite morphology control through oxide surface passivation.

A key feature of the surface passivation strategy outlined here is the ability to preserve the shape of the template throughout all stages of shell growth. In order to test this further, we prepared ZnO as nanowires and star-shaped templates for ZIF-8 formation. (Figure S25, S26) Reaction of these ZnO architectures with MeIm in the presence of C_{12}Gua leads to the formation of ZnO@ZIF-8 core-shell composites as evidenced by PXRD (figure S27, S28), which fully retain the well-defined template morphology as confirmed by electron microscopy. (Figure 2)

We note that solvent also plays an important role, and that ZnO to ZIF-8 conversion of more complex architectures is best conducted under aqueous conditions (Figure S29) as previously used for ZnO nanospheres (figure S2). In water the ZIF-8 shell deposited on ZnO microspheres is composed of much smaller crystals and conversion is lower than when MeOH is employed as solvent. (Figure S30-S32) This is consistent with a faster initial release of Zn(II) under aqueous conditions[20], as previously demonstrated for low levels of C_{12}Gua oxide surface coverage (figure S14; table S3). This is a favourable situation where the increase in nucleation over growth afforded in water leads to more rapid shell deposition than in MeOH under comparable conditions, and allows templates of more complex shape and smaller size to retain their morphology. By contrast, in a growth dominated process the intergrowth of larger ZIF-8 crystals would eventually mask the shape of the underlying template, and while not apparently a major factor for ZnO microspheres this becomes very important for non-spherical and down-sized oxide templates.

In practise, the amount of C_{12}Gua surfactant, metal:linker ratio and solvent need to be balanced in order to obtain the desired shape and required level of oxide-to-MOF conversion through fine-tuning of the chemical potential of the framework building blocks relative to the rate of framework growth[18-22]. In the present case we clearly demonstrate that using a C_{12}Gua amphiphile that nanoscale ZnO and templates with more complex morphology can also be directly transformed to core-shell ZnO@ZIF-8 composites in water only, whereas all previous studies tend to use alcohol or aqueous-DMF mixtures[18-22]. This opens the possibility to include biomolecules in future complex MOF-based composite materials templated by oxides.

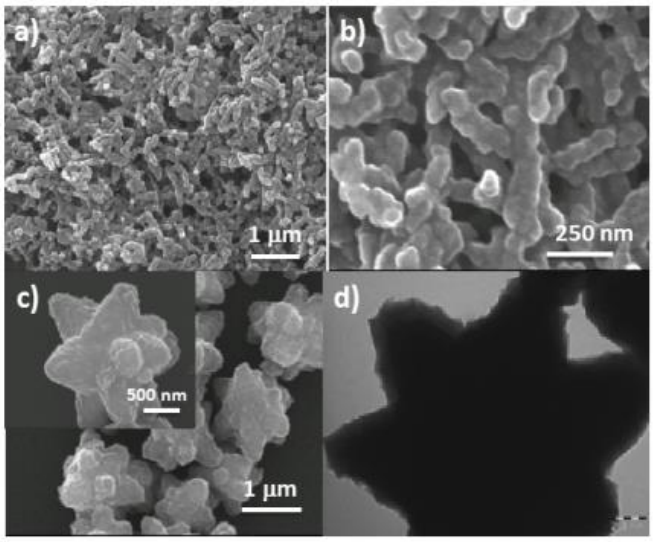

Figure 2. Microscopy images of non-spherical ZnO@ZIF-8 composites prepared in the presence of C_{12}Gua. (a) and (b) SEM images of ZnO@ZIF-8 composite nanowires. (c) SEM images of star-shaped ZnO@ZIF-8 composites and d) TEM image of a single star-shaped composite showing the core-shell nature of the structure. Scale bar in (d) = 200 nm.

The ZnO@ZIF-8 core-shell structures provide an easy route to hollow ZIF-8 architectures via selective etching of the amphoteric ZnO core following protection of the external surface with polyvinylpyrrolidone (PVP). (Figure 3) Taking advantage of the base stability of ZIF-8[14], the oxide core can be effectively and rapidly removed from the composites by soaking in 2M KOH for 10-15 mins. While related template-etch strategies to prepare ZIF-8 capsules from functionalised colloidal polystyrene templates[26] and access to Pd@ZIF-8 yolk-shell structures from sacrificial coatings of Cu_2O on Pd nanoparticles[27] have been reported, we believe this is the first time an oxide has been used both as metal-source and a hard post-synthetically etchable template for the formation of MOF-based hollow structures.

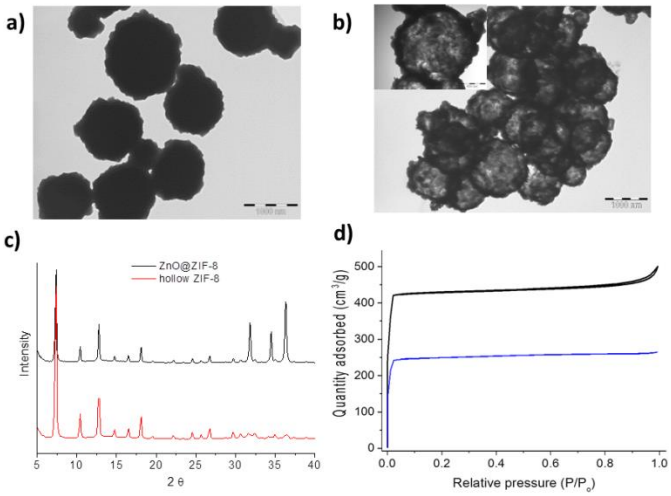

Figure 3. Characterisation data following selective base etching of the ZnO core from ZnO@ZIF-8 composite microspheres. (a) TEM image of the ZnO@ZIF-8 core-shell composite microspheres; scale bar = 1 µm. (b) TEM images of the hollow ZIF-8 microspheres after etching of the composite in (a) with 2M KOH; scale bar = 1 µm and inset 500 nm. (c) PXRD data of the as-made ZnO@ZIF-8 composites (black) and following etching (red) confirming removal of the oxide core. (d) Nitrogen adsorption isotherms measured at 77 K before (blue) and after (black) etching with KOH.

Figure 3a,b shows TEM images of well-defined hollow ZIF-8 microspheres prepared via selective base etching of ZnO@ZIF-8 core-shell composites, and the corresponding SEM images are presented in figure S33. This further confirms the core-shell nature of the as-made composite microspheres.

PXRD reveals near complete removal of the oxide core without disruption to the ZIF-8 lattice. (Figure 3c) Oxide removal is also confirmed by TGA where mass losses following the etching process are consistent with the composition of the starting composites, and final residual masses match those expected for ZIF-8 alone. (Figure S34) After etching of the ZnO@ZIF-8 microspheres a type I microporous isotherm is observed and the BET surface area increases from 1047 m^2/g for the composite to 1810 m^2/g for the hollow capsules as the oxide core is removed. (Figure 3d) Complementary characterisation data for hollow star-shaped ZIF-8 architectures following selective base etching is shown in figures S35 – S37.

Furthermore, etching of those composites prepared using high levels of C_{12}Gua such as those shown in figure S14d, selectively removes the oxide particles to leave micron-sized bowl-like ZIF-8 crystals which contain large hollow cavities. (Figure S38) We note that similar hollow structures can be obtained by direct face-selective etching of ZIF-8 crystals using pH-adjusted solutions of xylenol orange[28] dependent on the morphology of the crystals used.

Coating the ZnO@ZIF-8 composites in PVP is crucial to maintaining the shape in all of the resulting hollow structures during base etching. In the absence of PVP, there is significant disruption to the ZIF-8 shells leading to break up of the microspheres and large numbers of free ZIF-8 crystals. (Figure S39) This is analogous to the acid-induced etching of Prussian Blue mesocrystals, where adsorbed layers of PVP significantly reduce the rate of etching on the outer surface leading to the controlled formation of hollow particles[29], and the PVP-stabilised template-free formation of MOF-5 derived hollow nanocages.[30] Further, the surface-functionalisation assisted etching of ZIF-8 using phenolic acids has recently been demonstrated[31].

To investigate the potential to include functional nanoparticles[13a, 32] into the composites using this approach, we also employed core-shell spherical Fe_3O_4@ZnO nanoparticles (NPs) of ~ 150 nm diameter (figure S40) and star-shaped AuNP@ZnO particles as templates. (Figure S41) The corresponding Fe_3O_4@ZnO@ZIF-8 and AuNP@ZnO@ZIF-8 ternary composites were prepared in water with C_{12}Gua, and in both cases PXRD confirms the partial transformation of the oxide coating into ZIF-8. (Figure S42, S43)

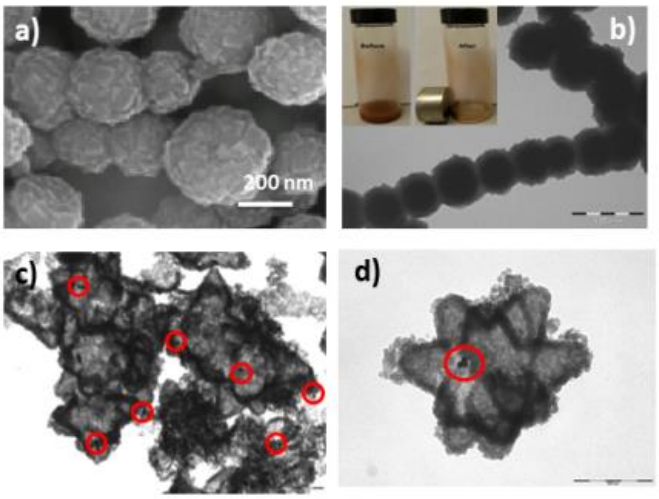

Figure 4. (a) and (b) SEM and TEM images of Fe_3O_4@ZnO@ZIF-8 ternary composite spheres. Scale bar in (b) = 500 nm. The inset in (b) highlights their attraction to a permanent magnet. (c) and (d) TEM images of yolk-shell AuNP@ZIF-8 star-shaped architectures following selective etching of the ZnO component from AuNP@ZnO@ZIF-8 composites. Scale bar in (d) = 500 nm. Au NPs are circled in red.

SEM and TEM images of Fe_3O_4@ZnO@ZIF-8 (Figure 4a, b, S44) reveal an increase in diameter as the thickness of the ZIF-8 shell increases with reaction time, and the magnetite core is easily visible by TEM. While the corresponding microscopy images for AuNP@ZnO@ZIF-8 indicate the star-shape morphology of the template was retained and a shell of ZIF-8 is clearly formed (Figure S45), the small size of the Au NPs (~ 45 nm) relative to the thickness of the ZnO makes these difficult to visualise. However, the oxide component of AuNP@ZnO@ZIF-8 can be facilely and selectively etched away using KOH to generate star-shaped AuNP@ZIF-8 yolk-shell architectures (figure 4c, d) where the hollow nature allows the encapsulated Au NPs to be located. Removal of the oxide is further confirmed by PXRD and TGA (figure S43, S46), the latter indicating that the yolk-shell structures contain 6 wt% Au. Selective etching of Au NPs from AuNP@ZIF-8 composites

using solutions of KI/I_2 has previously been reported as a strategy to introduce mesoporosity into MOFs where the size, shape and location of the mesopores can be carefully controlled[33]. This opens up the possibility for sequential etching procedures of the oxide-derived ternary MOF-composites described here to target specific functionality, tailor porosity and introduce complex morphologies. We also note that ammonia etching of Prussian Blue crystals followed by annealing leads to well-defined hollow nanocages of a mixed oxide with improved electrocatalytic properties[34], which could indicate that MOF-based cage architectures could be further transformed or act as templates for a range of nanomaterials or carbons with enhanced properties arising from their well-defined morphology.[35]

The recovery of dyes from aqueous solution is an important goal as many are toxic compounds that make their way into wastewater flows[36]. Adsorption using activated carbon[37], oxides[38] and sustainable materials derived from waste[36] have all been investigated for this purpose, including a number of MOFs[39]. For the latter it is noted that adsorption properties and recovery can be improved by appropriate configuration or by using MOF-based composites[40]. In this study, we have thus investigated the potential of the ZnO@ZIF-8 composites for the adsorption and separation of rhodamine B (RhB) from aqueous solution (Figure 5a) in order to determine any enhancements arising from the core-shell structure and microspherical morphology.

Compared to ZIF-8 or the oxide alone, ZnO@ZIF-8 has an enhanced adsorption for RhB (figure 5b) as determined by UV-vis spectroscopy of the supernatant following removal of the solid composite by centrifugation. The adsorption efficiency of the composite is 87.0%, which is higher than ZIF-8 (38.0%) or ZnO (5.8%) alone when 4 mg of the solids is each added to a 0.02 mM aqueous solution of RhB for 1 hr. The adsorption of RhB also increases with the amount of composite added, but for ZnO and ZIF-8 RhB adsorption remains relatively constant with increasing solid content (Figure S47) indicating the relatively poor adsorption properties of the individual components.

The surface adsorption of RhB on ZIF-8 particles has previously been reported, and since RhB is larger than the pores of ZIF-8 the external surface area is important to uptake. For example, RhB adsorption on ZIF-8 nanoparticles with adsorption efficiencies up to 20% have been observed whereas almost no uptake for micron-sized crystals of the framework is recorded[41]. However, a solvent-assisted extraction procedure using binary water-solvent mixtures was found to significantly increase extraction kinetics over ZIF-8 crystals alone, where adsorption efficiencies of > 90% were achieved within a few minutes exposure.[42] Addition of a small quantity of a non-miscible solvent confines the hydrophobic ZIF-8 crystals into the dispersed phase, where the higher density of the (dispersed) droplets causes them to sink, significantly improving the interfacial contact with the dye-containing aqueous phase. By contrast bulk ZIF-8 tended to float on the surface of the solution, impairing dye adsorption even under stirring conditions.

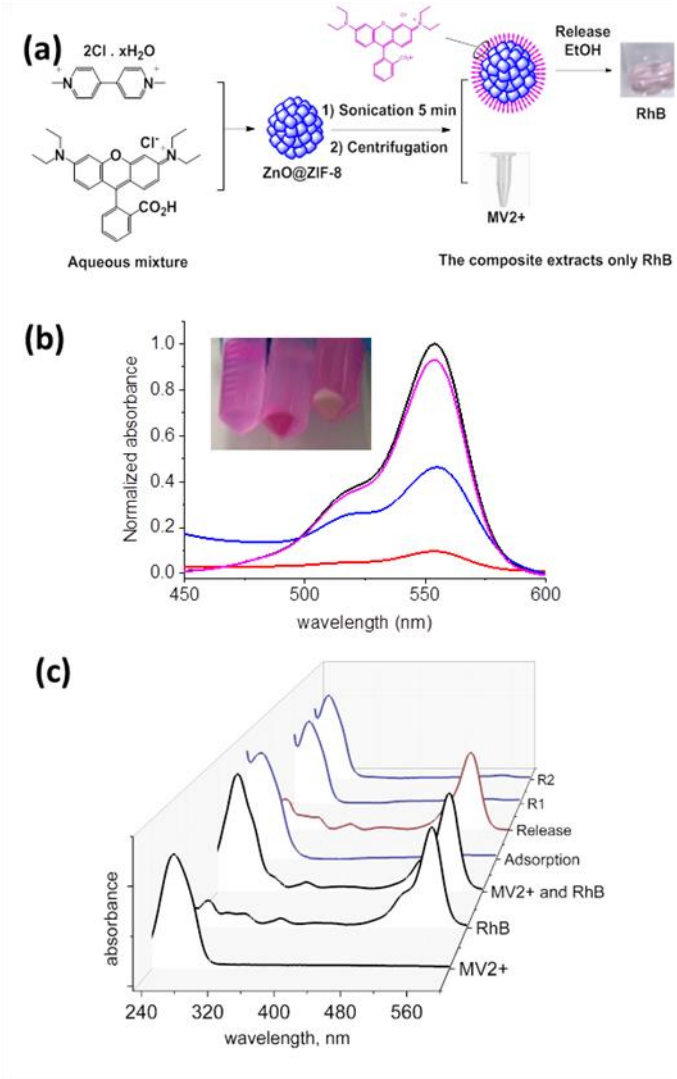

Figure 5. (a) Schematic representation of selective dye adsorption from aqueous solution using ZnO@ZIF-8 composite microspheres. (b) Normalized UV-Vis absorption spectra of aqueous supernatants following RhB (black) adsorption demonstrating enhanced uptake for the composite (red) compared to ZIF-8 (blue) or the ZnO template (pink) alone. The inset shows a photograph following centrifugation to remove the solid from solution following RhB adsorption L-R: ZIF-8, ZnO@ZIF-8 composite and ZnO. (c) UV-Vis absorption spectra demonstrating selective adsorption of RhB over MV^{2+} from aqueous solution, showing full recovery of RhB following release from the composite surface with EtOH. The second and third RhB adsorption cycles are denoted R1 and R2.

An analogous effect is clearly seen for the ZnO@ZIF-8 composite, where the increased density of the ZnO core plays a similar role to the dispersed phase reported by Maya et al.[42], such that the structure and microspherical configuration provide a more effective surface for RhB adsorption. (Figure 5b, inset) Under the conditions tested above, the RhB uptake capacity is 6.3 mg/g of composite microspheres or 13 mg/g if this is normalized to the contents of ZIF-8 in the microspheres (~ 50% on average). This is a 4.6-fold increase in adsorption

capacity over ZIF-8 alone (2.85 mg/g under identical conditions) and is similar to the enhancement observed by Maya prior to optimisation of ZIF-8 particle size[42], and clearly demonstrates that appropriate processing of MOF-based composites is important for enhanced dye adsorption. Although the uptake by the ZnO@ZIF-8 microspheres has not been optimised with respect to pH, RhB concentration, composite dose and ionic strength[39c], it is not expected to reach the levels observed for those MOFs with much larger pores that are able to accommodate the RhB as a guest in addition to surface adsorption[43].

Water adsorption isotherms demonstrate that the surface of ZIF-8 is hydrophobic in nature[44], such that coatings of ZIF-8 on zeolite 5A to form core-shell zeolite@ZIF-8 composites, can significantly improve CO_2 separation performance through dynamic hydrophobic hindrance effects[45]. The pH of the as-made RhB solution is 5.27, indicating that the fluorophore exists largely in its neutral form, consistent with the observed absorption maximum at 553 nm (figure 5b). While RhB is a water soluble dye, its somewhat limited solubility and octanol/water partition coefficient (Table S5) indicate this does have a degree of hydrophobicity compared to other water soluble dyes. We therefore attribute the strong tendency for the composite to adsorb RhB to hydrophobic effects between the dye and the ZIF-8 shell[46], although it is also clear that the microspherical core-shell configuration and increased density of the ZnO@ZIF-8 composite also have an important role to play as described above.

To evaluate whether this enhanced surface adsorption could be used to separate RhB from aqueous dye mixtures, we added the ZnO@ZIF-8 microspheres to a 1:4 mixture of RhB and methyl viologen (MV^{2+}). UV-vis data recorded on the dye solution after 5 mins exposure to 15 mg of the composite reveals that RhB is selectively removed with an adsorption efficiency of 94.8%, as evidenced by the absence of the RhB absorption band at ~ 553 nm while that associated with MV^{2+} (~ 248 nm) remains. (Figure 5c) The recovered solid is intensely pink in colour and the adsorbed RhB can be easily and quantitatively recovered by soaking in EtOH. (Figure 5c) Following recovery of the adsorbed dye, the composite microspheres can be reused for two further cycles of adsorption and release without loss of RhB capacity. (Figure 5c, S48) Highly selective adsorption of RhB using ZnO@ZIF-8 from a solution containing a 100-fold excess of MV^{2+} is also demonstrated (figure S49), further confirming the very strong affinity this dye has for the surface of the composite. Similar results from the 1:100 RhB/MV^{2+} dye solution are obtained when Fe_3O_4@ZnO@ZIF-8 is employed (figure S50), and since the ternary composite is attracted to a permanent magnet this further simplifies the recovery process[47]. (Figure S51)

Separation of methyl orange (MO) from MV^{2+} is also possible using the ZnO@ZIF-8 composite, where MO adsorption efficiencies of 57% are observed from the mixture. This is lower than for RhB in the presence of MV^{2+} and overall recovery is also reduced due to the decreased solubility of MO in EtOH, which lessens capacity in subsequent adsorption cycles. (Figure S52) The poor overall adsorption of MV^{2+} with the surface of the ZnO@ZIF-8 composite microspheres appears largely dependent on its reduced hydrophobicity (Table S5), although an electrostatic contribution cannot be ruled out when considering selectivity with respect to the anionic MO.

Overall, the observed recyclability and selectivity, coupled with the microsphere configuration, strongly suggests that the ZnO@ZIF-8 based composites could be used as adsorbents for the solid-phase extraction of dyes and wider classes of organic compounds[48].

Conclusions

The surface-passivation of ZnO using a guanidinium-based amphiphile permits the formation of well-defined ZnO@ZIF-8 core-shell architectures that fully retain the shape of the oxide template upon reaction with MeIm. The key feature of this strategy is the ability to fine-tune the balance between Zn(II) release from the oxide and subsequent coordination by regulating surface-coverage of C_{12}Gua. This is applicable across a range of reaction conditions which allows composite shape and ZIF-8 conversion level to be carefully controlled. The potential of the prepared ZnO@ZIF-8 microspheres for selective dye removal from aqueous solution has also been demonstrated, which is enhanced by the core-shell configuration of the composite.

By coating functional nanoparticles in ZnO and using C_{12}Gua, ternary composites of complex architecture are also accessible including star-shaped AuNP@ZnO@ZIF-8 materials. The oxide cores of the composites can be selectively etched away with base to leave hollow ZIF-8 and Au@ZIF-8 yolk-shell structures. We anticipate that the surface-passivation strategy will be applicable to other MOF systems, in particular where core-shell composite formation directly from the oxide or other ceramic phase has been hampered by rapid dissolution of the template. The preparation of continuous supported MOF thin films and membranes may also benefit by the additional control afforded by this method.

Experimental section

Materials

Zinc nitrate hexahydrate [$Zn(NO_3)_2{\cdot}6H_2O$], 2-methylimidazole (MeIm), poly(vinyl pyrrolidone) (PVP, MW = 40000), Sodium tetrachloroaurate(III) dihydrate, Cetyl trimethylammonium bromide (CTAB), sodium borohydride, dodecyl amine, 1*H*-Pyrazole-1-carboxamidine hydrochloride, $FeCl_3.6H_2O$, ethylene glycol (EG) , sodium acetate, trisodium citrate, Starch, NaOH, NH_4OH, $ZnCl_2$, Tetra ethylene glycol (TEG), 3-mercaptopropionic acid and Hexamethylenetetramine (HMTA) were all purchased from Sigma-Aldrich. DMF, EtOH, MeOH, potassium hydroxide (KOH) were purchased from Fisher. All chemicals were used without further purification.

Synthesis of mesoporous ZnO.

To a soluble starch (5 g) dissolved in boiling water (100 ml; milliQ water), was dropwise added $Zn(NO_3)_2.6H_2O$ (0.01 mol) dissolved in 10 ml of water until the starch solution becomes clear. The resulting solution was heated to 100 °C for 15 min

and then allowed to cool to 90 °C. The pH of this solution was adjusted to 8.5 with aqueous NH_4OH until a white, milk-like suspension was formed. After stirring for a further 30 min, the precipitate was left overnight and then isolated by centrifugation, washed with water and ethanol three times and dried (60 °C, 2 h). The isolated white product was transferred to a crucible, placed in a muffle furnace and calcined in air at 500 - 600 °C for 2 h to yield the mesoporous ZnO nanospheres.

Synthesis of ZnO nanospheres.

1.387 g (0.01mol) of $ZnCl_2$ powder was weighed and added to 100 ml of TEG and aged for a 2 day period. Separately, 0.8 g (0.02 mol) of NaOH pellets was dissolved in 100 ml of TEG under ageing for two days. The two solutions were mixed together at rt and heated at 90 °C for 2h while continuously stirring. The temperature was raised to 150 ^oC for 4h. 60ml of water was added to the precipitated solid, which was isolated by centrifugation and washed twice with distilled water and once with EtOH. Finally, 2g of PVP-40000 was added and left overnight to stabilise the spherical particles. Then centrifuged, washed with EtOH and air dried.

Synthesis of star-shape ZnO.

185 mg of $Zn(NO_3)_2.6H_2O$ was dispersed in 25 mL of distilled H_2O. The pH of the solution was adjusted to 12 with sNaOH, and the mixture was heated at 45 ^oC for 30 min. Finally, the precipitate was centrifuged, washed with H_2O and EtOH, and dried at 60 °C overnight.

Synthesis of nanowire ZnO.

3 g of PVP (MW 40 000) was dissolved in 180 mL of ethanol and then 0.75 g of $[Zn(OAc)_2].2H_2O$ was slowly added into the solution. The resulting mixture was stirred for several minutes, followed by addition of 4.5 g of NaOH. A turbid solution resulted and was stirred for a further 2 h before heating in an autoclave at 80 °C for 22 h. After cooling, the resulting solid was washed twice with water and finally once with EtOH before drying at rt.

Synthesis of 45 nm Au NPs.

Au NPs were synthesised by following the procedure reported by Yun et al.[49] Briefly, sodium tetrachloroaurate(III) dihydrate (12 mg, 0.029 mmol) was added to 10 mL of water containing 106 mg of CTAB (0.29 mmol). Next, 1 mL of an ice-cold water-solution of sodium borohydride (44 mg, 1.16 mmol) was added. After 3 h of stirring, 0.5 mL of this solution was added to a fresh water solution (20 mL) of 106 mg CTAB and 24 mg of sodium tetrachloroaurate(III) dihydrate (0.060 mmol). Then, 1 mL of ascorbic acid (16 mg, 0.09 mmol, AA : Au = 1.5) was added, and the mixture stirred for a further 30 min.

Synthesis of Fe_3O_4 NPs.

1.08 g of $FeCl_3{\cdot}6H_2O$ was first dissolved in 20 mL of EG under magnetic stirring. A clear yellow solution was obtained after stirring for 0.5 h. Then 1.8 g of sodium acetate (NaOAc) was added to this solution and stirred for a further 1 h. followed by addition of 0.25 g of trisodium citrate. The mixed solution was stirred for 5 h to form a homogeneous dispersion, then transferred into a Teflon-lined stainless-steel autoclave (50 mL capacity) and heated at 200 °C for 10 h. After cooling, the black magnetic particles were collected by a magnet and washed 3 times with EtOH. The product was then dried at rt.

Synthesis of star-shape Au@ZnO templates.

Star-shaped Au@ZnO composites were obtained by using the same procedure described for the star-shaped ZnO, but adding 1 mL of the as-synthesized Au NPs after dissolving the zinc nitrate in water.

Synthesis of Fe_3O_4@ZnO templates.

20mg of Fe_3O_4 was dispersed in 35 mL of water, to which was added 10µl of 3-mercaptopropionic acid and heated in an autoclave at 60^oC for 2h. The supernatant was removed and 7ml of water and 0.3mg of PVP-40000 added to the residue. After sonication, 1 mmol of Zn nitrate and 1 mmol of HMTA were added, the mixture sonicated for 3min then left in an oven at 90^oC for 3h. The solid was separated by a magnet and washed twice with EtOH before drying at rt.

Synthesis of Dodecylguanidinium Chloride (C_{12}Gua).

Dodecylamine (55 mmol) and 1H-pyrazole-1-carboxamidine hydrochloride (50 mmol) were dissolved in methanol (100 mL) and the solution stirred at 40 °C for 3 days. After this time, the solvent was removed and the crude reaction product purified by repeated recrystallization from acetone. Yield is > 90%.

Synthesis of ZnO@ZIF-8 and related composites.

In general, 50mg (0.61 mmol) of ZnO and 50 or 75mg (0.15 or 0.27 mmol, respectively) of C_{12}Gua were dissolved in 10ml of MeOH (or water) then stirred for 1h. After this time 1.5g (18.75 mmol) of MeIM was added giving a total Zn:MeIm ratio of 1:30. The reaction was allowed to occur for 3 days at rt or 60 °C. The resulting solids were recovered by centrifugation, washed three times with EtOH and then dried in air at rt. This general procedure was modified according to the amount of MeIm or C_{12}Gua outlined in the text, and the overall reaction time was also varied. When CTAB was employed, 75 mg was used in place of C_{12}Gua. For the nanoscale and star-shaped templates (including those containing Fe_3O_4 and Au NPs), the aqueous reaction was conducted for 24 hrs. After adding C_{12}Gua to the aqueous suspension of star-shaped and nanowire ZnO particles, the mixture was gently stirred for one hour before adding MeIm (to avoid destruction of the particles).

Selective etching of the ZnO core.

20 mg of the desired composite was dispersed in 5 mL of distilled H_2O and sonicated for 5 min. 50 mg of PVP (MW = 40000) was added and the mixture was stirred at rt for 1 h, followed by the addition of 5 mL of 2M KOH. After standing for 10 min without stirring, 10 mL of EtOH was added. Finally, the material was centrifuged and washed with H_2O and EtOH several times followed by air drying at rt.

Dye adsorption and release.

Standard aqueous dye solutions of RhB and MV^{2+} were prepared at a concentration of 0.02 mM. To assess the affinity of RhB for the ZnO@ZIF-8 composite, amounts of 2, 3 and 4mg were added to the solution and sonicated for 1 hr prior to filtration and UV analysis. This experiment was repeated with ZnO and ZIF-8 only. Adsorption efficiencies were determined by integrating the areas under the curves as a fraction of the initial concentration of RhB. For separation studies, a mixture

was prepared using 4ml of RhB solution and 16ml of MV^{2+}, set at a 1:4 ratio (1:2 in the case of MO) in order to have the same UV-intensity. 15mg of the composite microspheres were added to 3mL of the mixed solution and sonicated for 5min. After solids were removed by centrifugation, the supernatant was measured by UV-vis spectroscopy. For the recyclability, 3ml of the stock mixture solution was added to the same portion of composite after previously releasing the adsorbed RhB with EtOH.

Characterisation.

X-Ray diffraction data were collected on a Bruker D2 phaser in the angular range 2 θ = 5-40° employing a Ni Kβ filter (detector side) producing Cu (Kα1/Kα2) radiation.

N_2 adsorption/desorption isotherms were measured at 77 K using a Micromeritics 3-Flex Surface Characterization Analyzer after the sample was first degassed at 120 °C overnight. Surface areas were determined by the BET method in an appropriate pressure range. UV-visible spectra were obtained using a Shimadzu 2700 spectrophotometer on the aqueous or ethanolic supernatants following dye adsorption by (or release from) the composites. Thermogravimetric analysis (TGA) was performed using a TG 209 F1 Libra (Netzsch) and the sample was heated from room temperature to 900 °C at a rate of 10 °C min-1 under an air atmosphere. SEM measurements were made on a JEOL JSM 6500F field-emission scanning electron microscope at an accelerating voltage of 10 kV. The SEM sample was prepared by placing a drop of microsphere suspension in absolute ethanol on a silica wafer attached to an aluminium substrate, dried under vacuum, then sputter-coated with a thin conductive gold layer. TEM measurements were taken with a Hitachi H7000 electron microscope working at 80 kV equipped with a digital camera. The TEM sample was prepared by firstly placing a drop of sample suspension in absolute ethanol on a carbon grid, then drying overnight in air.

Acknowledgements

We gratefully acknowledge the European Research Council for funding under contract number ERC-2010-StG-258613-BIOMOF.

Notes and references

† These authors contributed equally to this work.

1 a) H. Furukawa, K. E. Cordova, M. O'Keeffe, O. M. Yaghi, *Science* 2013, **341**, 974; b) C. Janiak, J. K. Vieth, *New J. Chem*. 2010, **34**, 2366; c) S. Kitagawa, R. Kitaura, S. Noro, *Angew. Chem, Int. Ed*. 2004, **43**, 2334; d) G. Fe´rey, *Chem. Soc. Rev*. 2008, **37**, 191.

2 a) A. Corma, H. Garcia, F. X. Llabre i Xamena, *Chem. Rev*. 2010, **110**, 4606; b) J. Liu, L. Chen, H. Cui, J. Zhang, L. Zhang, C.-Y. Su, *Chem. Soc. Rev*. 2014, **43**, 6011.

3 a) B. Li, H. Wang, B. Chen, *Chem. Asian J*. 2014, **9**, 1474; b) B. Van de Voorde, B. Bueken, J. Denayer, D. De Vos, *Chem. Soc. Rev*. 2014, **43**, 5766.

4 a) L. Wang, Y. Han, X. Feng, J. Zhou, P. Qi, B. Wang, *Coord. Chem. Rev*. 2016, **307**, 361; b) S.-L. Li, Q. Xu, *Energy Environ. Sci.* 2013, **6**, 1656.

5 a) M. Gimenez-Marques, T. Hidalgo, C. Serre, P. Horcajada, *Coord. Chem. Rev*. 2016, **307**, 342; b) J. Della Rocca, D. Liu, W. Lin. *Acc. Chem. Res*. 2011, **44**, 957.

6 R. Ricco, C. Pfeiffer, K. Sumida, C. J. Sumby, P. Falcaro, S. Furukawa, N. R. Champness, C. J. Doonan, *CrystEngComm* 2016, DOI: 10.1039/C6CE01030J.

7 a) S. Furukawa, J. Reboul, S. Diring, K. Sumida, S. Kitagawa, *Chem. Soc. Rev*. 2014, **43**, 5700; b) D. Bradshaw, S. El-Hankari, L. Lupica-Spagnolo, *Chem. Soc. Rev*. 2014, **43**, 5431; c) A. Carne-Sanchez, I. Imaz, K. C. Stylianou, D. Maspoch, *Chem. Eur. J.* 2014, **20**, 5192.

8 a) D. Bradshaw, A. Garai, J. Huo, *Chem. Soc. Rev*. 2012, **41**, 2344; b) Q.-L. Zhu, Q. Xu, *Chem. Soc. Rev*. 2014, **43**, 5468.

9 a) Y. Hu, X. Dong, J. Nan, W. Jin, X. Ren, N. Xu, Y. Moo Lee, *Chem. Commun*. 2011, **47**, 737; b) A. Kasik, J. James, Y. S. Lin, *Ind. Eng. Chem. Res*. 2016, **55**, 2831; c) H. Guo, G. Zhu, I. J. Hewitt, S. Qiu, *J. Am. Chem. Soc.* 2009, **131**, 1646.

10 a) X. Zhao, S. Liu, Z. Tang, H. Niu, Y. Cai, W. Meng, F. Wu. J. P. Giesy, *Sci. Rep*. 2015, **5**, 11849; b) Z. Xiong, Y. Ji, C. Fang, Q. Zhang, L. Zhang, M. Ye, W. Zhang, H. Zou, *Chem. Eur. J*. 2014, **20**, 7389; c) K. Khaletskaya, J. Reboul, M. Meilikhov, M. Nakahama, S. Diring, M. Tsujimoto, S. Isoda, F. Kim, K. Kamei, R. A. Fischer, S. Kitagawa, S. Furukawa, *J. Am. Chem. Soc*. 2013, **135**, 10998.

11 J. Reboul, S. Furukawa, N. Horike, M. Tsotsalas, K. Hirai, H. Uehara, M. Kondo, N. Louvain, O. Sakata and S. Kitagawa, *Nat. Mater.* 2012, **11**, 717.

12 E. Zanchetta, L. Malfatti, R. Ricco, M. J. Styles, F. Lisi, C. J. Coghlan, C. J. Doonan, A. J. Hill, G. Brusatin, P. Falcaro, *Chem. Mater*. 2015, **27**, 690.

13 a) P. Falcaro, R. Ricco, A. Yazdi, I. Imaz, S. Furukawa, D. Maspoch, R. Ameloot, J. D. Evans, C. J. Doonan, *Coord. Chem. Rev*. 2016, **307**, 237; b) J. Aguilera-Sigalat, D. Bradshaw, *Coord. Chem. Rev*. 2016, **307**, 267.

14 K. S. Park, Z. Ni, A. P. Coˆte´, J. Y. Choi, R. Huang, F. J. Uribe-Romo, H. K. Chae, M. O'Keeffe, O. M. Yaghi, *Proc. Nat. Acad. Sci*. 2006, **103**, 10186.

15 B. Chen, Z. Yang, Y. Zhu, Y. Xia, *J. Mater. Chem. A* 2014, **2**, 16811.

16 a) I. Stassen, N. Campagnol, J. Fransaer, P. Vereecken, D. De Vos, R. Ameloot, *CrystEngComm* 2013, **15**, 9308; b) H. Al-Kutubi, A. Dikhtiarenko, H. Reza Zafarani, E. J. R. Sudhölter, J. Gascon, L. Rassaei, *CrystEngComm* 2015, **17**, 5360; c) K. Khaletskaya, S. Turner, M. Tu, S. Wannapaiboon, A. Schneemann, R. Meyer, A. Ludwig, G. Van Tendeloo, R. A. Fischer, *Adv. Funct. Mater*. 2014, **24**, 4804; d) S. M. Meckler, C. Li, W. L. Queen, T. E. Williams, J. R. Long, R. Buonsanti, D. J. Milliron, B. A. Helms, *Chem. Mater*. 2015, **27**, 7673.

17 I. Stassen, M. Styles, G. Grenci, H. Van Gorp ,W. Vanderlinden, S. De Feyter, P. Falcaro, D. De Vos, P. Vereecken, R. Ameloot, *Nat. Mater*. 2016, **15**, 304.

18 a) X. Wang, J. Liu, S. Leong, X. Lin, J. Wei, B. Kong, Y. Xu, Z.-X. Low, J. Yao, H. Wang, *ACS Appl. Mater. Inter.* 2016, **8**, 9080; b) B. Yu. F. Wang, W. Dong, J. Hou, P. Lu, J. Gong, *Mater. Lett.* 2015, **156**, 50.

19 H. Tian, H. Fan, M. Li, L. Ma, *ACS Sens*. 2016, **1**, 243

20 W.-W. Zhan, Q. Kuang, J.-Z. Zhou, X.-J. Kong, Z.-X. Xie, L.-S. Zheng, *J. Am. Chem. Soc.* 2013, **135**, 1926.

21 L. Lin, T. Zhang, H. Liu, J. Qiu, X. Zhang, *Nanoscale* 2015, **7**, 7615.

22 S. Li, W. Zhang, Y. Zhu, Q. Zhao, F. Huo, *Cryst. Growth Des*. 2015, **15**, 1017.

23 a) Y. Yue, Z.-A. Qiao, X. Li, A. J. Binder, E. Formo, Z. Pan, C. Tian, Z. Bi, S. Dai, *Cryst. Growth Des*. 2013, **13**, 1002; b) L. Maserati, S. M. Meckler, C. Li, B. A. Helms, *Chem. Mater.* 2016, **28**, 1581.

24 H. Bakrudeen, J. Tsibouklis, B. R. Reddy, *J. Nanopart. Res*. 2013, **15**, 1.

25 Y. Pan, D. Heryadi, F. Zhou, L. Zhao, G. Lestari, H. Su, Z. Lai, *CrystEngComm* 2011, **13**, 6937.

26 a) F. Zhang, Y. Wei, X. Wu, H. Jiang, W. Wang, H. Li, *J. Am. Chem. Soc*. 2014, **136**, 13963; b) H. J. Lee, W. Cho, M. Oh, *Chem. Commun*. 2012, **48**, 221.

27 C.-H. Kuo, Y. Tang, L.-Y. Chou, B. T. Sneed, C. N. Brodsky, Z. Zhao, C.-K. Tsung, *J. Am. Chem. Soc*. 2012, **134**, 14345.

28 C. Avci, J. Arinez-Soriano, A. Carne-Sanchez, V. Guillerm, C. Carbonell, I. Imaz, D. Maspoch, *Angew. Chem. Int. Ed*. 2015, **54**, 14417.

29 M. Hu, S. Furukawa, R. Ohtani, H. Sukegawa, Y. Nemoto, J. Reboul, S. Kitagawa, Y. Yamauchi, *Angew. Chem. Int. Ed*. 2012, **51**, 984.
30 Z. Zhang, Y. Chen, X. Xu, J. Zhang, G. Xiang, W. He, X. Wang, *Angew. Chem. Int. Ed*. 2014, **53**, 429.
31 M. Hu, Y. Ju, K. Liang, T. Suma, J. Cui, F. Caruso, *Adv. Funct. Mater*. 2016, DOI: 10.1002/adfm.201601193.
32 Y. Liu, Z. Tang, *Adv. Mater*. 2013, **25**, 5819.
33 W. Zhang, Y. Liu, G. Lu, Y. Wang, S. Li, C. Cui, J. Wu, Z. Xu, D. Tian, W. Huang, J. S. DuCheneu, W. Wei, H. Chen, Y. Yang, F. Huo, *Adv. Mater*. 2015, **27**, 2923.
34 L. Han, X.-Y. Yu, X. W. Lou, *Adv. Mater*. 2016, **28**, 4601.
35 P. Pachfule, D. Shinde, M. Majumder, Q. Xu, *Nature Chem*. 2016, **8**, 718.
36 M. T. Yagub, T. K. Sen, S. Afroze, H. M. Ang, *Adv. Colloid Inter. Sci*. 2014, **209**, 172.
37 G. Mezohegyi, F. P. van der Zee, J. Font, A. Fortuny, A. Fabregat, *J. Environ. Management* 2012, **102**, 148.
38 a) P. Basnit, Y. Zhao, *J. Mater. Chem. A* 2014, **2**, 911; b) C.-H. Huang, K.-P. Chang, H.-D. Ou, Y.-C. Chiang, C.-F. Wang, *Micro Meso. Mater*. 2011, **141**, 102.
39 a) A. A. Adeyemo, I. O. Adeoye, O. S. Bello, *Toxic. Environ. Chem*. 2012, **94**, 1846; b) X.-L. Hu, F.-H. Liu, H.-N. Wang, C. Qin, C.-Y. Sun, Z.-M. Su, F.-C. Liu, *J. Mater. Chem. A* 2014, **2**, 14827; c) M. S. Tehrani, .R. Zare-Dorabei, *RSC Adv*. 2016, **6**, 27416; d) H. Guo, F. Lin, J. Chen, F. Li, W. Weng, *Appl. Organometal. Chem*. 2015, **29**,12.
40 a) A.-X. Yan, S. Yao, Y.-G. Li, Z.-M. Zhang, Y. Lu, W.-L. Chen, E.-B. Wang, *Chem. Eur. J*. 2014, **20**, 6927; b) Y. Xiong, F.Ye, L. Zhang, S. Shen, L. Su, S. Zhao, *RSC Adv*. 2015, **5**, 5164.
41 X. Fan, W. Wang, W. Li, J. Zhou, B. Wang, J. Zheng, X. Li, *ACS Appl. Mater. Interfaces* 2014, **6**, 14994.
42 F. Maya, C. Palomino Cabello, S. Clavijo, J. M. Estela, V. Cerd`a, G. Turnes Palomino, *RSC Adv*. 2015, **5**, 28203.
43 R. Grunker, V. Bon, A. Heerwig, N. Klein, P. Muller, U. Stoeck, I. A. Babuin, U. Mueller, I. Senkovska, S. Kaskel, *Chem. Eur. J*. 2012, **18**, 13299.
44 a) P. Küsgens, M. Rose, I. Senkovska, H. Fröde, A. Henschel, S. Siegle, S. Kaskel. *Micro. Meso. Mater*. 2009, **120**, 325; b) K. Zhang, R. P. Lively, M. E. Dose, A. J. Brown, C. Zhang, J. Chung, S. Nair, W. J. Koros, R. R. Chance, *Chem. Commun*. 2013, **49**, 3245.
45 F. Gao, Y. Li, Z. Bian, J. Hu, H. Liu, *J. Mater. Chem. A* 2015, **3**, 8091
46 Z. Hasan, S. H. Jhung, *J. Hazard. Mater*. 2015, **283**, 329.
47 J. Zheng, C. Cheng, W.-J. Fang, C. Chen, R.-W. Yan, H.-X. Huai, C.-C. Wang, *CrystEngComm* 2014, **16**, 3960.
48 a) A. Ahmed, M. Forster, J. Jin, P. Myers, H. Zhang, *ACS Appl. Mater. Interfaces* 2015, **7**, 18054; b) M. del Rio, C. P. Cabello, V. Gonzalez, F. Maya, J. B. Parra, V. Cerda, G. T. Palomino, *Chem. Eur J*. 2016, **22**, 11770.
49 Y. Yun, H. Shuhua, Z. Guangju, Z. Lijie, L. Xingliang, Z. Chao, H.Shaoming, *Nanoscale* **2013**, *5*, 11808.